

Research Article: New Research | Disorders of the Nervous System

Disruption of VGLUT1 in cholinergic medial habenula projections increases nicotine self-administration

https://doi.org/10.1523/ENEURO.0481-21.2021

Cite as: eNeuro 2021; 10.1523/ENEURO.0481-21.2021

Received: 12 November 2021 Accepted: 21 November 2021

This Early Release article has been peer-reviewed and accepted, but has not been through the composition and copyediting processes. The final version may differ slightly in style or formatting and will contain links to any extended data.

Alerts: Sign up at www.eneuro.org/alerts to receive customized email alerts when the fully formatted version of this article is published.

Copyright © 2021 Souter et al.

This is an open-access article distributed under the terms of the Creative Commons Attribution 4.0 International license, which permits unrestricted use, distribution and reproduction in any medium provided that the original work is properly attributed.

Disruption of VGLUT1 in cholinergic medial habenula

2 projections increases nicotine self-administration

3 Abbreviated title: Ventral MHb VGLUT1 loss increases nicotine intake

4

5 Elizabeth A. Souter¹; Yen-Chu Chen²; Vivien Zell¹; Valeria Lallai²; Thomas Steinkellner¹; William

6 S. Conrad¹; William Wisden³; Kenneth D. Harris⁴; Christie D. Fowler²; Thomas S. Hnasko^{1,5}

- 7
- ⁸ ¹Department of Neurosciences, University of California, San Diego, La Jolla, CA 92093, USA
- 9 ²Department of Neurobiology and Behavior sciences, University of California, Irvine, Irvine, CA
- 10 92697, USA
- ¹¹ ³Department of Life Sciences & UK Dementia Research Institute, Imperial College London,
- 12 London SW7 2AZ, UK
- ¹³ ⁴Institute of Neurology, University College London, Queen Square, London WC1N 3BG, UK
- ¹⁴ ⁵Research Service VA San Diego Healthcare System, San Diego, CA 92161, USA

15

16 AUTHOR CONTRIBUTIONS

- 17 TSH designed research. EAS, YC, VZ, VL, TS, WSC, CDF and TSH performed research and
- 18 analyzed data. WW and KDH contributed unpublished reagents/analytical tools. EAS, WSC,
- 19 CDF and TSH wrote the paper, with input from all authors.
- 20
- 21 Correspondence and material requests should be addressed to T.S.H.
- 22 (thnasko@health.ucsd.edu; 9500 Gilman Drive, La Jolla CA 92093; 858 822 0672)

23

24 Figures = 5

- 25 Abstract = 236 words
- 26 Significance statement = 108 words
- 27 Introduction = 650 words
- 28 Discussion = 1089 words
- 29
- 30 **DISCLOSURE**
- 31 Authors report no conflict of interest.
- 32

33 FUNDING

- 34 This work was supported by funding from the Tobacco-Related Disease Research Program
- 35 (340144) and NIH National Institute on Drug Abuse (R01DA036612, K99DA046514,
- 36 DP1DA039658) NIA (K99AG059834), and NIDCD (R01DC009947-01).

2

1 ABSTRACT

2

3	Cholinergic projections from the medial habenula (MHb) to the interpeduncular nucleus (IPN)
4	have been studied for their complex contributions to nicotine addiction and have been
5	implicated in nicotine reinforcement, aversion, and withdrawal. While it has been established
6	that MHb cholinergic projections co-release glutamate, no direct evidence has demonstrated a
7	role for this glutamate projection in nicotine consumption. In the present study, a novel floxed
8	Slc17a7 (VGLUT1) mouse was generated and used to create conditional knockout (cKO) mice
9	that lack VGLUT1 in MHb cholinergic neurons. Loss of Slc17a7 expression in ventral MHb
10	cholinergic neurons was validated using fluorescent in situ hybridization, and
1	immunohistochemistry was used to demonstrate a corresponding reduction of VGLUT1 protein
12	in cholinergic terminals in the IPN. We also used optogenetics-assisted electrophysiology to
13	evoke excitatory post-synaptic currents in IPN and observed a reduction of glutamatergic
14	currents in the cKO, supporting the functional disruption of VGLUT1 in MHb to IPN synapses.
15	cKO mice exhibited no gross phenotypic abnormalities and displayed normal thigmotaxis and
16	locomotor behavior in the open-field assay. When trained to lever press for food, there was no
17	difference between control and cKO. However, when tested in a nicotine self-administration
18	procedure we found that the loss of VGLUT1-mediated glutamate co-release led to increased
19	responding for nicotine. These findings indicate that glutamate co-release from ventral MHb
20	cholinergic neurons opposes nicotine self-administration, and provide additional support for
21	targeting this synapse to develop potential treatments for nicotine addiction.
22	
23	Significance statement: Excitatory projections from the medial habenula (MHb) to

24 interpeduncular nucleus (IPN) have been studied for their role in mediating the aversive

25 properties of nicotine and nicotine intake behaviors. Although these projections are known to co-

26 release acetylcholine and glutamate, the present study is the first investigation of a function for

this glutamate signaling in nicotine consumption. We demonstrate that a loss of VGLUT1 from cholinergic MHb neurons promotes increased nicotine self-administration in mice. Thus, we outline a role for glutamate release from MHb cholinergic projections in mediating the aversive properties of nicotine, expanding our knowledge of the neurobiology underlying nicotine consumption and identifying a possible substrate for therapeutic intervention.

32

33 INTRODUCTION

34

35 Despite decades of research demonstrating the negative consequences of smoking and 36 emerging evidence on harmful effects of electronic cigarettes, the use of tobacco products 37 persists. In the United States, nicotine use among adolescents has increased in recent years. 38 For instance, in 2019, 23% of middle and high school students reported use of a nicotine-39 containing product in the past 30 days, up from 9% in 2014 (Kasza et al., 2017; Wang et al., 40 2019). As the main psychoactive and addictive compound, nicotine remains at the forefront of 41 this continuing public health crisis (Cooper & Henderson, 2020; Dani & Heinemann, 1996; 42 Mansvelder & McGehee, 2002; Wittenberg et al., 2020). 43

44 Nicotine mediates its psychoactive effect by acting on nicotinic acetylcholine receptors 45 (nAChRs) in the brain. Within the mesolimbic circuit, including ventral tegmental area dopamine 46 neuron projections to nucleus accumbens, activation of nAChRs contribute to the rewarding 47 effect of nicotine (Akers et al., 2020; Calabresi et al., 1989; Grieder et al., 2019; Liu et al., 2012; 48 Mansvelder & McGehee, 2000; Peng et al., 2017; Pons et al., 2008; Pontieri et al., 1996). 49 Conversely, the excitatory projection from medial habenula (MHb) to interpeduncular nucleus 50 (IPN) has been identified as a key substrate upon which nicotine actions contribute to nicotine 51 aversion (Antolin-Fontes et al., 2015; Antolin-Fontes et al., 2020; Elayouby et al., 2021; Fowler

52 & Kenny, 2011, 2014; Fowler et al., 2011b; Frahm et al., 2015b; Frahm et al., 2011; Salas et al.,
53 2009; Tuesta et al., 2017).

54

55 Both MHb and IPN express high levels of several nAChR subunits which modulate excitability 56 and neurotransmission within this projection (Dineley-Miller & Patrick, 1992; Marks et al., 1992; 57 McGehee et al., 1995; Perry et al., 2002; Salas et al., 2004; Shih et al., 2014). Mice lacking α5-58 containing nAChRs self-administered significantly more nicotine at high (typically aversive) 59 doses, an effect which was normalized by viral expression of α5 nAChR subunit in the MHb or 60 IPN, suggesting that α5-containing nAChRs in this circuit are necessary for nicotine aversion 61 (Fowler et al., 2011b). Additionally, overexpression of β 4 nAChR subunit led to enhanced MHb 62 activity and a strong aversive response to nicotine, which was abolished by disruption of the $\alpha 5$ nAChR subunit in MHb (Frahm et al., 2011). More recently, it has been shown that knockdown 63 of the α3 nAChR subunit in either the MHb or IPN increased nicotine intake in rats (Elayouby et 64 65 al., 2021). Together these data suggest that nAChRs containing the α 5, α 3, and β 4 subunits 66 mediate aversive signaling through the MHb→IPN. Further, IPN projections to laterodorsal 67 tegmentum (LDTg) are also strongly modulated by nicotine, and inhibiting this projection is 68 sufficient to block nicotine aversion (Wolfman et al., 2018). Together, these findings establish 69 the importance of MHb projections to IPN in modulating intake of nicotine and encoding its 70 aversive properties.

71

MHb-IPN projections are topographically organized, with ventral MHb cholinergic projections
targeting central IPN and Substance P-containing projections from dorsal MHb targeting lateral
IPN (Contestabile et al., 1987; Herkenham & Nauta, 1979; Quina et al., 2017). The cholinergic
ventral MHb expresses nAChRs and has been particularly implicated in nicotine aversion
(Dineley-Miller & Patrick, 1992; Fowler et al., 2011b; Frahm et al., 2011; Harrington et al., 2016;

77 Marks et al., 1992; Perry et al., 2002; Shih et al., 2014). However, these neurons also express 78 vesicular glutamate transporter 1 (VGLUT1) and can thus co-release both ACh and glutamate 79 (Aizawa et al., 2012; Frahm et al., 2015b; Ren et al., 2011), raising the question of what the 80 glutamate signal from MHb may contribute to nicotine intake. To address this question, we 81 made a new conditional VGLUT1 mouse line and used it to generate conditional knock-out 82 (cKO) mice that lack VGLUT1 in ventral MHb cholinergic neurons. We showed that cKO mice 83 have reduced glutamate transmission in MHb projections to IPN and that cKO mice displayed 84 increased intravenous (IV) nicotine self-administration, consistent with a role for VGLUT1-85 mediated glutamate co-release at this circuit in opposing nicotine intake.

86

87 METHODS

88

89 Animals

Mice were used in accordance with the University of California, San Diego and the University of California, Irvine Institutional Animal Care and Use Committees. BAC transgenic Kiaa1107-Cre mice were obtained from GENSAT through the MMRRC (#034692-UCD). Kiaa-Cre mice were bred hemizygously with C57Bl/6J wildtype mice (Jackson Laboratory, 000664). VGLUT2-IRES-Cre (*Slc17a6^{Cre}*) knock-in mice were ordered from Jackson Laboratory (#028863) and bred homozygously or to C57BL6/J wildtype mice. All experiments were done in adult mice (aged greater than 8 wks) and in both males and females in approximately equal proportion.

97

98 VGLUT1 conditional allele

99 To generate VGLUT1-floxed mice (*Slc17a7^{flox}*), a targeting vector containing two loxP sites

100 flanking Slc17a7 exons 4-7 and an FRT-flanked neomycin (Neo) resistance cassette was

101 electroporated into C57BI/6-derived ES cells. Antibiotic (G418)-resistant colonies were selected,

102 isolated, and amplified. The amplified clones were screened for homologous recombination at

103 the SIc17a7 locus by PCR. Southern blot analysis was used to confirm both 3' and 5' 104 homologous recombination. Blastocysts were isolated from pregnant C57BI/6J-Tyr^{c-2J}/J (albino 105 C57BI/6) females, injected with one of six validated ES cell clones, and implanted into pseudo-106 pregnant females. Chimeric males were bred to C57BI/6 females with constitutive expression of 107 FLP recombinase to excise the Neo cassette in F1 offspring. F1 mice were crossed to C57Bl/6, 108 excision was confirmed by PCR and Southern blot, and these F2 mice were used to establish the VGLUT1 floxed line (Slc17a7^{flox}). To generate conditional knock-out mice (Kiaa^{Cre}; 109 SIc17a7^{/lox/flox}), Kiaa^{Cre} mice were bred to homozygous SIc17a7^{/lox/flox} and resulting heterozygotes 110 (Kiaa^{Cre}; Slc17a7^{+//lox}) were then bred to homozygous Slc17a7^{flox//lox} mice. cKO mice used for 111 112 these studies were generated from 8 different breeder cages using 16 breeder mice. Mice were 113 group housed and maintained on a 12-hour light-dark cycle. Food and water were available ad 114 libitum except where noted.

115

116 Stereotactic surgery

117 For intracranial injections, mice (>4 weeks) were deeply anesthetized with isoflurane, placed in 118 a stereotaxic frame (Kopf), and bilaterally injected with AAV1-Ef1a-DIO-ChR2:mCherry (2 x 119 10^12, UNC Gene Therapy Center) into the MHb (LM = -1.15, AP = -1.58, DV = -2.42 and -2.00, 120 20° angle; right: LM = +0.95, AP = -1.58, DV = -2.42 and -2.00, 20° angle; mm relative to 121 Bregma). Two 150nL aliquots were given per hemisphere at 100 nl/min using pulled glass 122 pipettes (Nanoject III, Drummond Scientific). Analgesic was given before and at least one day 123 after surgery (Carprofen, Zoetis, 5 mg/kg s.c.). Mice were monitored daily for 5 d after surgery 124 and allowed to recover for at least 21 d before histological processing or 28 d before 125 electrophysiological recordings.

126

127 Immunohistochemistry

128 Mice were deeply anesthetized with pentobarbital (200 mg/kg s.c., VetOne) and transcardially 129 perfused for 2 min with ice-cold phosphate buffered saline (PBS) then for 8 min with ice-cold 4% 130 paraformaldehyde (PFA) at a rate of 5-6 ml/min. Brains were prepared as previously described 131 (Faget et al., 2018). Primary antibodies used: DsRed (Rabbit, 1:2000, Takara Bio, 132 RRID:AB_10013483), VGLUT1 (Guinea Pig, 1:2000, Synaptic Systems, RRID:AB_887878), 133 VGLUT2 (Rabbit, 1:1000, Synaptic Systems, RRID:AB_887883), ChAT (Goat, 1:200, Millipore, 134 RRID:AB_2079751). Secondary antibodies used (5ug/ml, Jackson ImmunoResearch): Alexa488 135 Donkey Anti-Goat (705-545-147, RRID:AB_2336933), Alexa 488 Donkey Anti-Guinea Pig (706-136 545-148, RRID:AB_2340472), Alexa594 Donkey Anti-Guinea Pig (706-585-148, 137 RRID:AB_2340474), Alexa 594 Donkey Anti-Rabbit (711-585-152, RRID:AB_2340621), 138 Alexa647 Donkey Anti-Rabbit (711-605-152, RRID:AB_2492288), Alexa647 Donkey Anti-Goat 139 (705-605-147, RRID:AB_2340437). Images were captured using a Zeiss AxioObserver Z1 140 epifluorescence microscope (10x 0.45NA, 20x 0.75NA, or 63x 1.4NA objective) and Zen 141 software. Zen software was used to set levels for each channel, and these parameters were 142 applied identically across sections. Adobe Photoshop was used to delineate the boundaries of 143 the IPN. Densitometry was done with Fiji/ImageJ using the Measure analysis tool. No 144 background subtraction was performed. Two to three sections were quantified per mouse; one 145 to three sections excluded per mouse due to tissue damage. No mice were excluded from 146 analysis following immunohistochemistry. 147

148Fluorescent in situ hybridization

149 Mice were deeply anesthetized with pentobarbital before cervical dislocation. Brains were

150 prepared as previously described (Faget et al., 2018). In situ hybridization was done using

- 151 RNAscope Multiplex Fluorescent Assay (Advanced Cell Diagnostics) according to manufacturer
- 152 specification. Slc17a7 (503511), ChAT (408731-C2), and Cre (312281-C3) were coupled to
- 153 Atto550, Alexa647, and Alexa488, respectively and counterstained with DAPI. Images were

captured using a Zeiss AxioObserver Z1 epifluorescence microscope and processed with Zen
software as described above. Adobe Photoshop was used to outline the MHb and densitometry
was done with the Fiji/ImageJ Measure analysis tool. No background subtraction was
performed. One to four sections were used per mouse; one to four sections excluded per mouse
due to tissue damage and/or signal indicative of cutting or labeling artifacts. No mice were
excluded from analysis.

160

161 **Open-Field Behavior**

Mice were placed in an Open Field (30 m) measuring 50x50 cm and their activity was recorded and analyzed using AnyMaze software (San Diego Instruments). The field was cleaned with 70% ethanol between sessions. The field was segmented into a 5x5 grid, with the innermost 9 squares designated as the center.

166

167 Operant Behavior

168 Operant testing and self administration studies were performed by experimenters blind to 169 genotype. Mice were fed 2-4 grams per mouse per day to achieve mild food-restriction to 85-170 90% of their free-feeding weight and were then trained to lever press for food pellets (grain-171 based, 20 mg, 5TUM, TestDiet) on a two-lever operant task across ascending fixed ratio (FR) 172 schedules from 1 up to 5 lever presses, as previously described (Fowler & Kenny, 2011). At the 173 start of the session, both levers were extended into the chamber and were present throughout 174 the 1-hr session. Responses on the active lever that met the FR criteria resulted in the delivery 175 of a food pellet, which was paired with a cue light for a 20-s time-out period, resulting in the final 176 reinforcement schedule of FR5TO20 for food training sessions 4-7. Responses on the inactive 177 lever were recorded but had no scheduled consequences. Testing was conducted 6-7 d/wk and 178 behavioral responses were recorded with a MedPC interface (Med Associates). Thereafter, 179 subjects were anesthetized (isoflurane) and catheterized as previously described (Chen et al.,

180	2018; Fowler & Kenny, 2011). The catheter tubing was passed subcutaneously from the
181	animal's back to the right jugular vein, a 1 cm length of catheter tip was inserted into the vein
182	and tied with surgical silk suture. Following surgery animals were allowed ≥48 hr to recover, and
183	were then provided 1 hr access to re-establish food responding under the FR5TO20 sec
184	schedule until the criteria of >30 pellets/session were again achieved. Mice were then
185	transitioned to respond for intravenous nicotine self-administration in lieu of food using the same
186	FR5TO20 sec, 1 hr daily sessions, 6-7 d/wk, at the training dose of nicotine (0.03
187	mg/kg/infusion) for 8 d. For all doses, nicotine (0.03 ml per infusion volume) was delivered
188	through tubing into the intravenous catheter by a Razel syringe pump (Med Associates). Based
189	on prior findings (Fowler & Kenny, 2011; Fowler et al., 2011a), mice typically achieve stable
190	responding for nicotine after ~5 days of acquisition, which can be evidenced by <20% variability
191	in responding between consecutive sessions. All mice were provided access to the acquisition
192	dose of nicotine for 8 days to allow for consistency in the total number of sessions, even though
193	many subjects acquired stable responding prior to 8 days. After achieving stable responding on
194	the 0.03 mg/kg/infusion dose, mice were transitioned to the moderate dose of 0.1
195	mg/kg/infusion nicotine for 5 d. This dose results in a similar levels of drug intake as that found
196	at higher doses with behavioral titration via self-administration and was used to further establish
197	baseline responding in between access to each subsequent varying dose (Fowler & Kenny,
198	2011). Next, the mice were provided access to either the low 0.01 mg/kg/infusion or high 0.4
199	mg/kg/infusion dose for 5d, and then re-established at baseline on 0.1 mg/kg/infusion for at
200	least 2 d, and thereafter given access to the counterbalanced doses of either 0.01 or 0.4
201	mg/kg/infusion for an additional 5 d. Following re-establishing baseline for at least 2 d, the mice
202	were provided access to respond for saline vehicle. The mean of the final 3 days on each dose
203	was calculated for each subject. Catheters were flushed daily with physiological sterile saline
204	solution (0.9% w/v) containing heparin (100 units/mL). Catheter integrity was verified with the
205	ultra-short-acting barbiturate anesthetic Brevital (2%, methohexital sodium, Eli Lilly) at the end

eNeuro Accepted Manuscript

206 of the study. One male mouse was excluded from nicotine self-administration behavior due to

207 excessive barbering injuries and one female excluded due to a leaky catheter.

208

209 Electrophysiological recordings

210 Recordings were performed by experimenters blind to genotype. Recordings were performed on

211 adult mice (7-12 wks) as previously described (Zell et al., 2020). mCherry-labeled MHb

212 terminals were visualized by epifluorescence and visually guided patch recordings were made

213 using infrared-differential interference contrast (IR-DIC) illumination (Axiocam MRm,

214 Examiner.A1, Zeiss). ChR2 was activated by flashing blue light (473 nm) through the light path

215 of the microscope using a light-emitting diode (UHP-LED460, Prizmatix) under computer

216 control. Neurons were held in voltage-clamp at -60 mV to record EPSCs in whole-cell

217 configuration and single-pulse photostimuli (5 ms or 1 s pulse width) were applied every 45 s

218 and 10 photo-evoked currents were averaged per neuron per condition. Stock solutions of

219 DNQX (10 mM in DMSO, Sigma) and mecamylamine hydrochloride (10 mM, Tocris) were

220 diluted 1,000-fold in ACSF and bath applied at 10 μ M. Current sizes were calculated by using

221 peak amplitude from baseline. Identification of glutamatergic or cholinergic currents relied

222 primarily on established kinetic properties, with pharmacology used to confirm in a subset of

223 cells (Frahm et al., 2015a; Ren et al., 2011).

224

225 Statistics

Data analysis was done using GraphPad Prism v9. Data were analyzed using t-test corrected
for multiple comparisons (Bonferroni-Sidak) (figures 1f, 1g, 1h, 2b, 2c, 2d), unpaired t-test (4c,
4d, 5e), and mixed-effects analysis (Sidak post hoc) (5a, 5b, 5c, 5d, 5f).

229

230 Table 1. Statistics Table

Figure	Type of test	Statistical data
1f	t-test (Bonferroni-Sidak)	dorsal: t(4)=0.004, p(adj)=0.99; ventral: t(4)=0.27, p(adj)=0.96
1g	t-test (Bonferroni-Sidak)	dorsal: t(4)=1.0, p(adj)=0.61; ventral: t(4)=6.4, p(adj)=0.006
1h	t-test (Bonferroni-Sidak)	dorsal: t(4)=0.79, p(adj)=0.72; ventral: t(4)=0.81, p(adj)=0.71
2b	t-test (Bonferroni-Sidak)	central: t(6)=0.89, p(adj)=0.65; lateral: t(6)=1.2, p(adj)=0.50
2c	t-test (Bonferroni-Sidak)	central: t(6)=5.2, p(adj)=0.004; lateral: t(6)=0.30, p(adj)=0.95
2d	t-test (Bonferroni-Sidak)	central: t(6)=0.31, p(adj)=0.94; lateral: t(6)=0.14, p(adj)=0.99
4c	unpaired t-test	t(14)=4.0, p=0.001
4d	unpaired t-test	t(13)=1.6, p=0.14
5a	mixed-effects analysis (Sidak)	main effect of segment, F(2.6,36)=30, p<0.0001; genotype, F(1,14)=0.12, p=0.73; segment x genotype interaction, F(5,70)=2.0, p=0.084
5b	mixed-effects analysis (Sidak)	main effect of segment, F(3.4,47)=1.1, p=0.38; genotype, F(1,14)=0.14, p=0.71; segment x genotype interaction, F(5,70)=0.19, p=0.97
5c	mixed-effects analysis (Sidak)	main effect of session, F(6,108)=72, p<0.0001; genotype, F(1,108)=0.10, p=0.75; lever, F(1,18)=243, p<0.0001; session x genotype, F(6,108)=0.90, p=0.50; session x lever, F(6,108)=74, p<0.0001; genotype x lever, F(1,108)=0.026, p=0.87; session x genotype x lever, F(6,108)=1.3, p=0.25
5d	mixed-effects analysis (Sidak)	main effect of session, $F(7,112)=38$, $p<0.0001$; genotype, $F(1,112)=11$, $p=0.001$; lever, $F(1,16)=111$, $p<0.0001$; session x genotype, $F(7,112)=1.8$, $p=0.099$; session x lever, $F(7,112)=33$, $p<0.0001$; genotype x lever, $F(1,112)=8.5$, $p=0.004$; session x genotype x lever, $F(7,112)=0.95$, $p=0.47$
5e	unpaired t-test	t(16)=2.3, p=0.035
5f	mixed-effects analysis (Sidak)	main effect of dose, F(4,64)=23, p<0.0001; genotype, F(1,16)=2.3, p=0.15; dose x genotype interaction, F(4,64)=3.5, p=0.012

231

232 **RESULTS**

233

234 Generation of *Slc17a7* conditional knock-out from ventral MHb

235

236 To target cholinergic neurons of the MHb we used the Kiaa1107-Cre (Kiaa^{Cre}) transgenic line

237 that has been used previously to disrupt Choline acetyltransferase (ChAT) expression in MHb

238 (Frahm et al., 2015b). The functional expression of Cre recombinase driven by Kiaa1107

regulatory elements was first validated by crossing to the Ai6 ZsGreen reporter (Madisen et al., 2010) to generate *Kiaa^{Cre}; Rosa26^{ZsGreen}* mice (**figure 1a**). Robust ZsGreen fluorescence was seen in MHb, with densest expression observed in ventral (basolateral and basomedial) MHb (**figure 1b**). Importantly, we also observed ZsGreen expression in VGLUT1-rich regions of cortex and hippocampus, but though some of these structures express VGLUT1 they are not known to project to IPN (expression pattern for the founder line KJ227 can be viewed throughout the rostral-caudal extent of brain at gensat.org).

246

247 To disrupt VGLUT1 expression, we generated a novel mouse line carrying a VGLUT1

conditional allele (*Slc17a7^{flox}*) with exons 4-7 flanked by loxP sites (**figure 1c**). We next crossed

249 SIc17a7^{flox} mice to Kiaa^{Cre} to generate the VGLUT1 conditional knockout (cKO, Kiaa^{Cre};

Slc17a7^{flox/flox}). We generated an RNAscope probe targeting exons 4-7 of *Slc17a7* and used this together with probes against a cholinergic marker (*Chat*) and *Cre recombinase* on sections from cKO and control (*Kiaa^{Cre}*) mice (**figure 1d-e**). The pattern of *Cre* expression was identical for both genotypes and similar to the pattern observed in the ZsGreen reporter cross, with robust expression in ventral MHb. *Chat* appeared unchanged across genotype and showed high overlap with *Cre.* Consistent with other reports, *Chat* expression was largely restricted to ventral MHb (Aizawa et al., 2012; Görlich et al., 2013; Oh et al., 1992; Trifonov et al., 2009).

257

258 Also consistent with other previous reports, Slc17a7 (VGLUT1) was expressed throughout the

259 MHb in controls (Aizawa et al., 2012; Barroso-Chinea et al., 2007; Fremeau et al., 2001;

260 Varoqui et al., 2002). However, the cKO showed a markedly different pattern (figure 1d-e). In

261 cKO mice, Slc17a7 (VGLUT1) expression was significantly reduced in ventral MHb (t(4)=6.4,

262 *p(adj)=0.006*), but was intact in dorsal (apical) MHb (*t(4)=1.0, p(adj)=0.61*) (**figure 1g**). There

was no difference in Cre expression in either dorsal (t(4)=0.004, p(adj)=0.99) or ventral

264 (t(4)=0.27, p(adj)=0.96) MHb (figure 1f). There was also no significant difference in Chat

expression in dorsal (*t*(*4*)=0.79, *p*(*adj*)=0.72) or ventral (*t*(*4*)=0.81, *p*(*adj*)=0.71) MHb between
groups (**figure 1h**). *Chat* expression was used to delineate the boundary between dorsal and
ventral MHb. These results indicate that our cKO successfully and selectively disrupted *Slc17a7*expression from Cre-expressing neurons in ventral MHb.

269

270 We next used immunohistochemistry to examine the expression of pre-synaptic cholinergic and 271 glutamatergic markers in the IPN, the major projection target of MHb (figure 2a). While the 272 expression of ChAT was unaffected in the cKO (figure 2b), the pattern of VGLUT1-labeled 273 fibers was markedly different depending on genotype and subregion. cKO mice had a significant 274 reduction of VGLUT1 expression compared to controls in central IPN (t(6)=5.2, p(adj)=0.004), 275 but no difference in VGLUT1 between genotypes was observed in lateral IPN (t(6)=0.30, 276 p(adj)=0.95) (figure 2c). Together, these data are concordant with our RNAscope data and 277 demonstrate the selective disruption of VGLUT1 from cholinergic MHb inputs that target the 278 central region of the IPN, which includes the caudal, dorsomedial, intermediate, and rostral 279 subnuclei. 280 281 We also examined VGLUT2-labeled fibers in the IPN to test whether the loss of VGLUT1 led to 282 changes in VGLUT2 expression. We detected no significant difference in VGLUT2 expression 283 between genotypes in either central IPN (t(6)=0.41, p(adj)=0.91) or lateral IPN (t(6)=0.25,

284 *p(adj)=0.96*) (**figure 2d**). These data argue against compensatory change in VGLUT2

285 expression following loss of VGLUT1 from cholinergic neurons in MHb.

286

287 Expression of Slc17a6 (VGLUT2) in IPN-projecting MHb neurons

288

289 The absence of Slc17a7/VGLUT1 expression in ChAT-expressing neurons of ventral MHb and

290 central IPN provides strong evidence for loss of VGLUT1-mediated glutamatergic co-release

291 from cholinergic MHb inputs in cKO mice. But while VGLUT1 has been implicated in mediating glutamate co-release from MHb cholinergic neurons (Aizawa et al., 2012; Frahm et al., 2015b; 292 293 Ren et al., 2011), there is also evidence that some MHb neurons express Slc17a6/VGLUT2 294 (Aizawa et al., 2012; Barroso-Chinea et al., 2007; Varoqui et al., 2002), consistent with the 295 presence of VGLUT2-labeled fibers that we observed in IPN (figure 2d). To directly test 296 whether *Kiaa^{Cre}*-expressing MHb cells also express *Slc17a6* (VGLUT2) we used RNAscope. 297 SIc17a6 was observed throughout the MHb (figure 3a), including in the ventral MHb where it 298 partially co-localized with Cre recombinase (Kiaa^{Cre}) (figure 3b).

299

300 The presence of MHb neurons co-expressing Cre and SIc17a6 (VGLUT2) in cKO mice raised 301 the question of whether this VGLUT2 population projected to IPN. We thus injected an Adenoassociated virus (AAV) into the MHb of S/c17a6^{Cre} (VGLUT2-Cre) mice (Vong et al., 2011) to 302 303 Cre-dependently express Channelrhodpsin-2 fused to a fluorescent tag (ChR2:mCherry). Three 304 weeks after surgery mCherry expression was found in MHb, as well as in surrounding areas of 305 lateral habenula (LHb) and paraventricular nucleus of the thalamus (PV) (figure 3c). mCherry-306 expressing fibers, presumably axon terminals from MHb, were also present in both central and 307 lateral IPN (figure 3d). These results indicate that at least some Kiaa^{Cre} cholinergic neurons in 308 MHb could express both VGLUT1 and VGLUT2, consistent with previous reports of 309 VGLUT1/VGLUT2 co-expression in MHb (Aizawa et al., 2012; Frahm et al., 2015b).

310

311 Disruption of VGLUT1 from ventral MHb neurons decreased evoked glutamate currents in

312 central IPN

313

We next tested how the loss of VGLUT1 from Cre-expressing ventral MHb cholinergic neurons affected glutamate transmission from terminals in central IPN. We expressed ChR2:mCherry in MHb as above, but now using *Kiaa*^{Cre} and cKO mice that lack VGLUT1 in these neurons (**figure**

317	4a). ChR2:mCherry expression was observed in MHb and IPN (figure 4b); recordings were
318	made from IPN neurons, with optogenetic stimulation of MHb terminals. Whole-cell voltage-
319	clamp was used to assess optogenetic-evoked excitatory postsynaptic currents (oEPSC) in
320	response to either a single pulse of blue light (5 ms) or train stimulation (5-ms pulses at 20Hz for
321	1 s). Single-pulse stimulation evoked fast glutamatergic oEPSCs (figure 4c) that were
322	significantly smaller but not eliminated in the cKO (unpaired t-test; t(14)=4.0, p=0.001). Residual
323	currents were presumably due to expression of VGLUT2 in some of the Cre-expressing
324	cholinergic neurons and were blocked by bath application of an AMPA-type glutamate receptor
325	antagonist (mean EPSC before DNQX 46 \pm 14 pA, after DNQX 1.5 \pm 1.5 pA; n=4). Train
326	stimulation led to a mixed response that contained both faster glutamatergic, as well as slower
327	cholinergic oEPSCs (figure 4d) that were blocked by a nicotinic acetylcholine receptor
328	antagonist (mean EPSC before mecamylamine 126 \pm 75 pA, after mecamylamine 24 \pm 1.5 pA;
329	n=3). While the variability in responses to train stimulation appeared higher in the cKO, no
330	significant difference in oEPSC amplitude was detected between genotypes in response to train
331	stimulation (unpaired t-test; t(13)=1.6, p=0.14), suggesting cholinergic transmission in the cKO
332	was largely intact, though more subtle functional changes cannot be excluded.
333	
334	Loss of MHb VGLUT1 increased nicotine self-administration
335	
336	Prior studies have implicated MHb cholinergic signaling to IPN in the aversive effects of nicotine
337	(Fowler & Kenny, 2011, 2014; Frahm et al., 2015b; Frahm et al., 2011; Harrington et al., 2016;

Salas et al., 2009), but the contribution of glutamate co-release from this circuit had not been
examined. We thus assessed the behavioral phenotype of littermate control and cKO mice. To

- 340 test gross locomotor and exploratory behavior, we assessed mice in the open-field test. No
- 341 significant differences were found between genotype in distance traveled (Mixed-effects

analysis; main effect of segment, F(2.6,36)=30, p<0.0001; genotype, F(1,14)=0.12, p=0.73;
segment x genotype interaction, F(5,70)=2.0, p=0.084) (figure 5a) or time spent in center (main

344 effect of segment, F(3.4,47)=1.1, p=0.38; genotype, F(1,14)=0.14, p=0.71; segment x genotype

345 interaction, *F*(5,70)=0.19, *p*=0.97) (figure 5b).

346

347 Next, control and cKO mice were trained to lever press for food pellets and each reward delivery 348 was paired with a cue-light for a 20 s timeout period (TO20). Across the initial 3 sessions, the 349 fixed ratio (FR) schedule increased from 1 to 5 lever presses, then mice were maintained on an 350 FR5 for an additional 3 sessions. No significant differences between genotypes were detected, 351 suggesting intact operant learning and lever discrimination in cKO mice (Mixed-effects analysis; 352 main effect of session, F(6,108)=72, p<0.0001; genotype, F(1,108)=0.10, p=0.75; lever, 353 F(1,18)=243, p<0.0001; session x genotype, F(6,108)=0.90, p=0.50; session x lever, 354 F(6,108)=74, p<0.0001; genotype x lever, F(1,108)=0.026, p=0.87; session x genotype x lever, 355 *F*(6,108)=1.3, *p*=0.25) (figure 5c).

356

357 After food training, intravenous catheters were implanted, and an acquisition dose of nicotine 358 (0.03 mg/kg/infusion) was introduced at the established FR5 TO20 schedule of reinforcement. 359 As previously observed with this protocol (Fowler & Kenny, 2011), both groups pressed initially 360 at a high rate similar to that observed with food reinforcement, which subsequently declined 361 across sessions to a steady-state rate of nicotine self-administration (figure 5d). cKO mice 362 engaged in consistently higher levels of nicotine self-administration across sessions at this dose 363 (Mixed-effects analysis; main effect of session, F(7, 112)=38, p<0.0001; genotype, F(1, 112)=11, p=0.001; lever, F(1,16)=111, p<0.0001; session x genotype, F(7,112)=1.8, p=0.099; session x 364 365 lever, F(7,112)=33, p<0.0001; genotype x lever, F(1,112)=8.5, p=0.004; session x genotype x 366 lever, F(7,112)=0.95, p=0.47). Compared to controls, cKO mice earned significantly more total 367 nicotine infusions in the first three test sessions (unpaired t-test; t(16)=2.3, p=0.035) (figure 5e). 368

369	To assess across a range of nicotine doses, a dose-response was then performed. While both
370	groups exhibited an inverted U-shaped dose-response, cKO mice showed a dose-dependent
371	increase in nicotine consumption compared to controls and this effect was most pronounced at
372	0.03 mg/kg/infusion dose (Mixed-effect analysis; main effect of dose, F(4,64)=23, p<0.0001;
373	genotype, <i>F</i> (1,16)=2.3, <i>p</i> =0.15; dose x genotype interaction, <i>F</i> (4,64)=3.5, <i>p</i> =0.012) (figure 5f).
374	Together, these results support the hypothesis that VGLUT1-mediated glutamate transmission
375	from MHb to IPN opposes nicotine self-administration.
376	
377	DISCUSSION
378	
379	The present study provides direct evidence for the role of glutamate release from MHb
380	cholinergic projections in opposing nicotine self-administration. Previous work on the role of

381 MHb->IPN projections in nicotine consumption has focused principally on cholinergic 382 transmission within this synapse. Indeed, nicotine facilitates glutamate release from MHb 383 terminals by activating pre-synaptic nAChRs (Girod et al., 2000; McGehee et al., 1995). Knock-384 down of $\alpha 5$ nAChR in MHb led to increased nicotine consumption in mice, as did blocking 385 glutamate transmission in IPN by microinjection of NMDA-receptor antagonist (Fowler et al., 386 2011b). More recently, targeted knock-down of α 3 nAChR subunit in either MHb or IPN was 387 shown to produce similar increases in nicotine intake (Elayouby et al., 2021). Global 388 overexpression of β4 nAChR subunit led to increased nicotine aversion, an effect reversed by 389 selective expression of α 5 nAChR subunit in MHb (Frahm et al., 2011). Together these data 390 indicate that nicotine acting on α 5-, α 3-, and β 4-containing nAChRs facilitates nicotine-mediated 391 excitatory transmission at MHb synapses in the IPN, which reduces nicotine-self administration.

392 Importantly, our data demonstrate that cKO of VGLUT1 in the MHb led to increased nicotine

393 self-administration, which is consistent with this framework and provides the first direct evidence

394 that release of glutamate from cholinergic MHb projections to IPN inhibits nicotine self-

395 administration.

396

397 MHb heterogeneity contributes to diverse effects

398 The MHb is a heterogenous structure composed of several distinct cell types, each capable of 399 releasing or co-releasing a variety of neurotransmitters or neuropeptides (Hashikawa et al., 400 2020; Wallace et al., 2020). For example, Fos data indicate that most MHb cell types are 401 activated by foot-shock stress (Hashikawa et al., 2020). On the other hand, activity in dorsal 402 MHb neurons, which are largely non-cholinergic, may play a role in positive reinforcement and 403 reward consumption (Hsu et al., 2016; Hsu et al., 2014). Further, stimulation of glutamatergic 404 septal inputs to MHb was anxiolytic, though different populations of MHb neurons were either 405 inhibited or excited by this manipulation (Otsu et al., 2019). Thus, different MHb cell types 406 appear to play opposing roles in mediating behaviors and affective states relevant to nicotine 407 consumption.

408

409 Disruption of glutamate transmission from MHb to IPN could increase nicotine self-410 administration if this glutamate signal opposes nicotine reward or mediates aspects of nicotine 411 aversion, though several lines of evidence favor the latter. For example, MHb projections to the 412 IPN mediate negative affective behaviors such as anxiety, aversion, and the expression and 413 extinction of fear memories (Fowler et al., 2011b; Otsu et al., 2019; Pang et al., 2016; Soria-414 Gomez et al., 2015; Wolfman et al., 2018; Yamaguchi et al., 2014; Zhang et al., 2016). In mice 415 undergoing nicotine withdrawal, optogenetic silencing of MHb inputs to IPN reduced marble-416 burying and increased time spent in the open arms of an elevated plus maze; microinjection of 417 NMDA antagonist in IPN recapitulated this effect and was also shown to reduce somatic signs 418 of withdrawal (Zhao-Shea et al., 2015; Zhao-Shea et al., 2013). Therefore, the loss of glutamate 419 release from cholinergic MHb projections in our study most likely led to increased nicotine 420 consumption by reducing its aversive properties, but future studies are necessary to lend 421 support to this conclusion. For example, while our study used a targeted genetic knock-out to 422 demonstrate a novel role for MHb→IPN glutamate release in decreasing nicotine self-423 administration, directly measuring or manipulating glutamate release at this synapse during 424 nicotine self-administration or conditioning assays would shed additional light and may help 425 distinguish whether the glutamate signal is facilitating nicotine aversion or opposing nicotine 426 reward.

427

428 Cholinergic/glutamatergic co-transmission from MHb to IPN

429 Previous reports have detailed activation of the central IPN by MHb projections via fast 430 glutamate-mediated currents, as well as by slower ACh-mediated currents (Frahm et al., 2015b; 431 McGehee et al., 1995; Ren et al., 2011). Histological assessments of VGLUT1 and the vesicular 432 ACh transporter (VAChT) have shown MHb axon terminals co-positive for these transporters, 433 and electron microscopy has identified vesicles at this synapse containing both vesicular 434 transporters (Aizawa et al., 2012; Frahm et al., 2015b; Ren et al., 2011). Our results are 435 consistent with prior works showing that dorsal MHb, which is not cholinergic, projects to lateral 436 IPN, while the cholinergic ventral MHb projects to central IPN (Contestabile et al., 1987; 437 Herkenham & Nauta, 1979; Quina et al., 2017). Further, our experiments show presence of both 438 SIc17a7/VGLUT1 and SIc17a6/VGLUT2 RNA transcripts in MHb, and that VGLUT2-expressing 439 MHb neurons can also project to both lateral and central IPN, consistent with prior findings 440 (Hashikawa et al., 2020; Qin & Luo, 2009; Wallace et al., 2020). In our VGLUT1 cKO animals, 441 the residual glutamate-mediated oEPSCs in IPN are most likely facilitated by expression of 442 VGLUT2. Nevertheless, cKO of VGLUT1 led to a large reduction in evoked glutamate currents 443 and to decreased nicotine intake, though disrupting both vesicular glutamate transporters might 444 produce an even larger effect which may be addressed in future studies.

445

446	Work by Frahm and colleagues used a similar conditional knockout approach to disrupt ChAT
447	expression in MHb and showed that this led to loss of nicotine withdrawal behaviors and loss of
448	nicotine conditioned place preference (Frahm et al., 2015b). Thus, despite both transmitters
449	exerting post-synaptic actions that are primarily excitatory, glutamate and ACh release from
450	MHb neurons appear to mediate different affective responses to nicotine – with acetylcholine
451	release necessary for nicotine-associated reward, and glutamate release signaling nicotine
452	aversion. This is perhaps more surprising given that these transmitters localize to an
453	overlapping pool of synaptic vesicles and synergistic effects on vesicle filling are supported by
454	data demonstrating that loss of ChAT/ACh reduces glutamate filling (Frahm et al., 2015b),
455	presumably because ACh uptake through VAChT dissipates the vesicular pH gradient and
456	increases the vesicular membrane potential that VGLUT relies on for packaging glutamate
457	(Hnasko & Edwards, 2012). And while we did not observe a reciprocal reduction in cholinergic
458	transmission in the VGLUT1 cKO, this may be due to high variability in detection of cholinergic
459	currents, or due to the presence of VGLUT2.

460

461 Conclusion

462 Nicotine consumption is shaped by a balance of its rewarding and aversive actions, thus our 463 understanding of the circuit mechanisms by which nicotine aversion is encoded is crucial for 464 developing effective therapeutics for nicotine addiction. Our findings demonstrate a role for 465 glutamate signals from MHb cholinergic projections to IPN in opposing nicotine self-466 administration and suggests that potentiating nicotine's effect on this circuit could be a useful 467 target for nicotine cessation therapies. Future work may also focus on dissecting the relative 468 roles of glutamate, ACh or other co-transmitters in this circuit on other aspects of nicotine 469 behavior or in mediating responses to other substances of abuse.

eNeuro Accepted Manuscript

470 **REFERENCES**

471

472 Aizawa, H., Kobayashi, M., Tanaka, S., Fukai, T., & Okamoto, H. (2012). Molecular 473 characterization of the subnuclei in rat habenula. The Journal of Comparative Neurology, 520(18), 4051-4066. https://doi.org/10.1002/cne.23167 474 475 Akers, A. T., Cooper, S. Y., Baumgard, Z. J., Casinelli, G. P., Avelar, A. J., & Henderson, B. J. 476 (2020). Upregulation of nAChRs and Changes in Excitability on VTA Dopamine and 477 GABA Neurons Correlates to Changes in Nicotine-Reward-Related Behavior. eNeuro, 478 7(5), ENEURO.0189-0120. https://doi.org/10.1523/eneuro.0189-20.2020 479 Antolin-Fontes, B., Ables, J. L., Görlich, A., & Ibañez-Tallon, I. (2015). The habenulo-480 interpeduncular pathway in nicotine aversion and withdrawal. Neuropharmacology, 96(Pt 481 B), 213-222. https://doi.org/10.1016/j.neuropharm.2014.11.019 482 Antolin-Fontes, B., Li, K., Ables, J. L., Riad, M. H., Görlich, A., Williams, M., Wang, C., Lipford, 483 S. M., Dao, M., Liu, J., Molina, H., Heintz, N., Kenny, P. J., & Ibañez-Tallon, I. (2020). 484 The habenular G-protein-coupled receptor 151 regulates synaptic plasticity and nicotine 485 intake. Proceedings of the National Academy of Sciences of the United States of 486 America, 117(10), 5502-5509. https://doi.org/10.1073/pnas.1916132117 487 Barroso-Chinea, P., Castle, M., Aymerich, M. S., Pérez-Manso, M., Erro, E., Tuñon, T., & 488 Lanciego, J. L. (2007). Expression of the mRNAs encoding for the vesicular glutamate 489 transporters 1 and 2 in the rat thalamus. Journal of Comparative Neurology, 501(5), 703-490 715. https://doi.org/10.1002/cne.21265

491	Calabresi, P., Lacey, M. G., & North, R. A. (1989). Nicotinic excitation of rat ventral tegmental
492	neurones in vitro studied by intracellular recording. British Journal of Pharmacology,
493	98(1), 135-140. https://doi.org/10.1111/j.1476-5381.1989.tb16873.x
494	Chen, E., Lallai, V., Sherafat, Y., Grimes, N. P., Pushkin, A. N., Fowler, J., & Fowler, C. D.
495	(2018). Altered Baseline and Nicotine-Mediated Behavioral and Cholinergic Profiles in
496	ChAT-Cre Mouse Lines. The Journal of Neuroscience, 38(9), 2177-2188.
497	https://doi.org/10.1523/jneurosci.1433-17.2018
498	Contestabile, A., Villani, L., Fasolo, A., Franzoni, M. F., Gribaudo, L., Øktedalen, O., & Fonnum,
499	F. (1987). Topography of cholinergic and substance P pathways in the habenulo-
500	interpeduncular system of the rat. An immunocytochemical and microchemical
501	approach. Neuroscience, 21(1), 253-270. <u>https://doi.org/10.1016/0306-4522(87)90337-X</u>
502	Cooper, S. Y., & Henderson, B. J. (2020). The Impact of Electronic Nicotine Delivery System
503	(ENDS) Flavors on Nicotinic Acetylcholine Receptors and Nicotine Addiction-Related
504	Behaviors. Molecules, 25(18), 4223. https://doi.org/10.3390/molecules25184223
505	
505	Dani, J. A., & Heinemann, S. (1996). Molecular and Cellular Aspects of Nicotine Abuse. Neuron,
506	16(5), 905-908. <u>https://doi.org/10.1016/s0896-6273(00)80112-9</u>
507	Dineley-Miller, K., & Patrick, J. (1992). Gene transcripts for the nicotinic acetylcholine receptor
508	subunit, beta4, are distributed in multiple areas of the rat central nervous system.
509	Molecular Brain Research, 16(3-4), 339-344. https://doi.org/10.1016/0169-
510	<u>328x(92)90244-6</u>
511	Elayouby, K. S., Ishikawa, M., Dukes, A. J., Smith, A. C. W., Lu, Q., Fowler, C. D., & Kenny, P.

512 J. (2021). α3* Nicotinic Acetylcholine Receptors in the Habenula-Interpeduncular

- 513 Nucleus Circuit Regulate Nicotine Intake. The Journal of Neuroscience, 41(8), 1779-514 1787. https://doi.org/10.1523/jneurosci.0127-19.2020 515 Faget, L., Zell, V., Souter, E., McPherson, A., Ressler, R., Gutierrez-Reed, N., Yoo, J. H., 516 Dulcis, D., & Hnasko, T. S. (2018). Opponent control of behavioral reinforcement by 517 inhibitory and excitatory projections from the ventral pallidum. Nature communications, 518 9(1). https://doi.org/10.1038/s41467-018-03125-y 519 Fowler, C. D., & Kenny, P. J. (2011). Intravenous nicotine self-administration and cue-induced 520 reinstatement in mice: Effects of nicotine dose, rate of drug infusion and prior 521 instrumental training. Neuropharmacology, 61(4), 687-698. 522 https://doi.org/10.1016/j.neuropharm.2011.05.012 523 Fowler, C. D., & Kenny, P. J. (2014). Nicotine aversion: Neurobiological mechanisms and 524 relevance to tobacco dependence vulnerability. Neuropharmacology, 76, 533-544. 525 https://doi.org/10.1016/j.neuropharm.2013.09.008 526 Fowler, C. D., Lu, Q., Johnson, P. M., Marks, M. J., & Kenny, P. J. (2011a). Habenular α5 527 nicotinic receptor subunit signalling controls nicotine intake. Nature, 471(7340), 597-601. 528 https://doi.org/10.1038/nature09797 529 Fowler, C. D., Lu, Q., Johnson, P. M., Marks, M. J., & Kenny, P. J. (2011b). Habenular α5 530 nicotinic receptor subunit signalling controls nicotine intake. Nature, 471(7340), 597-531 601. https://doi.org/10.1038/nature09797 532 Frahm, S., Antolin-Fontes, B., Görlich, A., Zander, J.-F., Ahnert-Hilger, G., & Ibañez-Tallon, I. 533 (2015a). An essential role of acetylcholine-glutamate synergy at habenular synapses in
 - 534 nicotine dependence. *eLife*, *4*, e11396. <u>https://doi.org/10.7554/elife.11396</u>

535	Frahm, S., Antolin-Fontes, B., Görlich, A., Zander, J. F., Ahnert-Hilger, G., & Ibañez-Tallon, I.
536	(2015b). An essential role of acetylcholine- glutamate synergy at habenular synapses in
537	nicotine dependence. eLife, 4, e11396. https://doi.org/10.7554/eLife.11396
538	Frahm, S., Ślimak, M. A., Ferrarese, L., Santos-Torres, J., Antolin-Fontes, B., Auer, S., Filkin,
539	S., Pons, S., Fontaine, J. F., Tsetlin, V., Maskos, U., & Ibañez-Tallon, I. (2011). Aversion
540	to Nicotine Is Regulated by the Balanced Activity of $\beta4$ and $\alpha5$ Nicotinic Receptor
541	Subunits in the Medial Habenula. Neuron, 70(3), 522-535.
542	https://doi.org/10.1016/j.neuron.2011.04.013
543	Fremeau, R. T., Troyer, M. D., Pahner, I., Nygaard, G. O., Tran, C. H., Reimer, R. J., Bellocchio,
544	E. E., Fortin, D., Storm-Mathisen, J., & Edwards, R. H. (2001). The expression of
545	vesicular glutamate transporters defines two classes of excitatory synapse. Neuron,
546	31(2), 247-260. https://doi.org/10.1016/S0896-6273(01)00344-0
547	Girod, R., Barazangi, N., Mcgehee, D., & Role, L. W. (2000). Facilitation of glutamatergic
548	neurotransmission by presynaptic nicotinic acetylcholine receptors. Neuropharmacology,
549	39(13), 2715-2725. https://doi.org/10.1016/s0028-3908(00)00145-3
550	Görlich, A., Antolin-Fontes, B., Ables, J. L., Frahm, S., Ślimak, M. A., Dougherty, J. D., &
551	Ibañez-Tallon, I. (2013). Reexposure to nicotine during withdrawal increases the
552	pacemaking activity of cholinergic habenular neurons. Proceedings of the National
553	Academy of Sciences of the United States of America, 110(42), 17077-17082.
554	https://doi.org/10.1073/pnas.1313103110
555	Grieder, T. E., Besson, M., Maal-Bared, G., Pons, S., Maskos, U., & Van Der Kooy, D. (2019).

556 β2* nAChRs on VTA dopamine and GABA neurons separately mediate nicotine aversion

557	and reward. Proceedings of the National Academy of Sciences, 116(51), 25968-25973.
558	https://doi.org/10.1073/pnas.1908724116
559	Harrington, L., Viñals, X., Herrera-Solís, A., Flores, A., Morel, C., Tolu, S., Faure, P.,
560	Maldonado, R., Maskos, U., & Robledo, P. (2016). Role of β4* Nicotinic Acetylcholine
561	Receptors in the Habenulo-Interpeduncular Pathway in Nicotine Reinforcement in Mice.
562	Neuropsychopharmacology, 41(7), 1790-1802. https://doi.org/10.1038/npp.2015.346
563	Hashikawa, Y., Hashikawa, K., Rossi, M. A., Basiri, M. L., Liu, Y., Johnston, N. L., Ahmad, O.
564	R., & Stuber, G. D. (2020). Transcriptional and Spatial Resolution of Cell Types in the
565	Mammalian Habenula. Neuron, 106(5), 743-758.e745.
566	https://doi.org/10.1016/j.neuron.2020.03.011
567	Herkenham, M., & Nauta, W. J. H. (1979). Efferent connections of the habenular nuclei in the
568	rat. Journal of Comparative Neurology, 187(1), 19-47.
569	https://doi.org/10.1002/cne.901870103
570	Hnasko, T. S., & Edwards, R. H. (2012). Neurotransmitter corelease: mechanism and
571	physiological role. Annu Rev Physiol, 74, 225-243. https://doi.org/10.1146/annurev-
572	physiol-020911-153315
573	Hsu, Y. W., Morton, G., Guy, E. G., Wang, S. D., & Turner, E. E. (2016). Dorsal Medial
574	Habenula Regulation of Mood-Related Behaviors and Primary Reinforcement by
575	Tachykinin-Expressing Habenula Neurons. eNeuro, 3(3).
576	https://doi.org/10.1523/ENEURO.0109-16.2016
577	Hsu, Y. W., Wang, S. D., Wang, S., Morton, G., Zariwala, H. A., de la Iglesia, H. O., & Turner, E.
578	E. (2014). Role of the dorsal medial habenula in the regulation of voluntary activity,

579	motor function, hedonic state, and primary reinforcement. J Neurosci, 34(34), 11366-
580	11384. https://doi.org/10.1523/JNEUROSCI.1861-14.2014
581	Kasza, K. A., Ambrose, B. K., Conway, K. P., Borek, N., Taylor, K., Goniewicz, M. L.,
582	Cummings, K. M., Sharma, E., Pearson, J. L., Green, V. R., Kaufman, A. R., Bansal-
583	Travers, M., Travers, M. J., Kwan, J., Tworek, C., Cheng, YC., Yang, L., Pharris-Ciurej,
584	N., van Bemmel, D. M., Backinger, C. L., Compton, W. M., & Hyland, A. J. (2017).
585	Tobacco-Product Use by Adults and Youths in the United States in 2013 and 2014. New
586	England Journal of Medicine, 376(4), 342-353. https://doi.org/10.1056/nejmsa1607538
587	Liu, L., Zhao-Shea, R., Mcintosh, J. M., Gardner, P. D., & Tapper, A. R. (2012). Nicotine
588	Persistently Activates Ventral Tegmental Area Dopaminergic Neurons via Nicotinic
589	Acetylcholine Receptors Containing $\alpha 4$ and $\alpha 6$ Subunits. <i>Molecular Pharmacology</i> ,
590	81(4), 541-548. https://doi.org/10.1124/mol.111.076661
591	Madisen, L., Zwingman, T. A., Sunkin, S. M., Oh, S. W., Zariwala, H. A., Gu, H., Ng, L. L.,
592	
	Palmiter, R. D., Hawrylycz, M. J., Jones, A. R., Lein, E. S., & Zeng, H. (2010). A robust
593	and high-throughput Cre reporting and characterization system for the whole mouse
594	brein Mature Maurensianes (2)(4) 422 440 bttps://doi.org/40.4020/pp.2407
	brain. Nature Neuroscience, 13(1), 133-140. <u>https://doi.org/10.1038/nn.2467</u>
595	Mansvelder, H. D., & McGehee, D. S. (2000). Long-Term Potentiation of Excitatory Inputs to
	Mansvelder, H. D., & McGehee, D. S. (2000). Long-Term Potentiation of Excitatory Inputs to
596	Mansvelder, H. D., & McGehee, D. S. (2000). Long-Term Potentiation of Excitatory Inputs to Brain Reward Areas by Nicotine. <i>Neuron</i> , <i>27</i> (2), 349-357. <u>https://doi.org/10.1016/s0896-</u>
	Mansvelder, H. D., & McGehee, D. S. (2000). Long-Term Potentiation of Excitatory Inputs to
596	Mansvelder, H. D., & McGehee, D. S. (2000). Long-Term Potentiation of Excitatory Inputs to Brain Reward Areas by Nicotine. <i>Neuron</i> , <i>27</i> (2), 349-357. <u>https://doi.org/10.1016/s0896-</u>
596 597	Mansvelder, H. D., & McGehee, D. S. (2000). Long-Term Potentiation of Excitatory Inputs to Brain Reward Areas by Nicotine. <i>Neuron</i> , <i>27</i> (2), 349-357. <u>https://doi.org/10.1016/s0896-6273(00)00042-8</u>
596 597 598	 Mansvelder, H. D., & McGehee, D. S. (2000). Long-Term Potentiation of Excitatory Inputs to Brain Reward Areas by Nicotine. <i>Neuron</i>, <i>27</i>(2), 349-357. <u>https://doi.org/10.1016/s0896-6273(00)00042-8</u> Mansvelder, H. D., & McGehee, D. S. (2002). Cellular and synaptic mechanisms of nicotine

602 treatment. The Journal of Neuroscience, 12(7), 2765-2784. 603 https://doi.org/10.1523/jneurosci.12-07-02765.1992 604 McGehee, D. S., Heath, M. J. S., Gelber, S., Devay, P., & Role, L. W. (1995). Nicotine 605 enhancement of fast excitatory synaptic transmission in CNS by presynaptic receptors. 606 Science, 269(5231), 1692-1696. https://doi.org/10.1126/science.7569895 607 Oh, J. D., Woolf, N. J., Roghani, A., Edwards, R. H., & Butcher, L. L. (1992). Cholinergic 608 neurons in the rat central nervous system demonstrated by in situ hybridization of 609 choline acetyltransferase mRNA. Neuroscience, 47(4), 807-822. 610 https://doi.org/10.1016/0306-4522(92)90031-V 611 Otsu, Y., Darcq, E., Pietrajtis, K., Matyas, F., Schwartz, E., Bessaih, T., Abi Gerges, S., 612 Rousseau, C. V., Grand, T., Dieudonne, S., Paoletti, P., Acsady, L., Agulhon, C., Kieffer, 613 B. L., & Diana, M. A. (2019). Control of aversion by glycine-gated GluN1/GluN3A NMDA 614 receptors in the adult medial habenula. Science, 366(6462), 250-254. 615 https://doi.org/10.1126/science.aax1522 616 Pang, X., Liu, L., Ngolab, J., Zhao-Shea, R., McIntosh, J. M., Gardner, P. D., & Tapper, A. R. 617 (2016). Habenula cholinergic neurons regulate anxiety during nicotine withdrawal via 618 nicotinic acetylcholine receptors. Neuropharmacology, 107, 294-304. 619 https://doi.org/10.1016/j.neuropharm.2016.03.039 620 Peng, C., Engle, S. E., Yan, Y., Weera, M. M., Berry, J. N., Arvin, M. C., Zhao, G., Mcintosh, J. 621 M., Chester, J. A., & Drenan, R. M. (2017). Altered nicotine reward-associated behavior 622 following α4 nAChR subunit deletion in ventral midbrain. PLOS ONE, 12(7), e0182142. 623 https://doi.org/10.1371/journal.pone.0182142

624	Perry, D. C., Xiao, Y., Nguyen, H. N., Musachio, J. L., Dávila-Garcí, M. I., & Kellar, K. J. (2002).
625	Measuring nicotinic receptors with characteristics of $\alpha 4\beta 2$, $\alpha 3\beta 2$ and $\alpha 3\beta 4$ subtypes in
626	rat tissues by autoradiography. Journal of Neurochemistry, 82(3), 468-481.
627	https://doi.org/10.1046/j.1471-4159.2002.00951.x
628	Pons, S., Fattore, L., Cossu, G., Tolu, S., Porcu, E., Mcintosh, J. M., Changeux, J. P., Maskos,
629	U., & Fratta, W. (2008). Crucial Role of $\alpha 4$ and $\alpha 6$ Nicotinic Acetylcholine Receptor
630	Subunits from Ventral Tegmental Area in Systemic Nicotine Self-Administration. Journal
631	of Neuroscience, 28(47), 12318-12327. https://doi.org/10.1523/jneurosci.3918-08.2008
632	Pontieri, F. E., Tanda, G., Orzi, F., & Chiara, G. D. (1996). Effects of nicotine on the nucleus
633	accumbens and similarity to those of addictive drugs. Nature, 382(6588), 255-257.
634	https://doi.org/10.1038/382255a0
635	Qin, C., & Luo, M. (2009). Neurochemical phenotypes of the afferent and efferent projections of
636	the mouse medial habenula. Neuroscience, 161(3), 827-837.
637	https://doi.org/10.1016/j.neuroscience.2009.03.085
638	Quina, L. A., Harris, J., Zeng, H., & Turner, E. E. (2017). Specific connections of the
639	interpeduncular subnuclei reveal distinct components of the habenulopeduncular
640	pathway. Journal of Comparative Neurology, 525(12), 2632-2656.
641	https://doi.org/10.1002/cne.24221
642	Ren, J., Qin, C., Hu, F., Tan, J., Qiu, L., Zhao, S., Feng, G., & Luo, M. (2011). Habenula
643	"Cholinergic" Neurons Corelease Glutamate and Acetylcholine and Activate
644	Postsynaptic Neurons via Distinct Transmission Modes. Neuron, 69(3).
645	https://doi.org/10.1016/i.neuron.2010.12.038

646	Salas, R., Pieri, F., & De Biasi, M. (2004). Decreased signs of nicotine withdrawal in mice null
647	for the β 4 nicotinic acetylcholine receptor subunit. Journal of Neuroscience, 24(45),
648	10035-10039. https://doi.org/10.1523/JNEUROSCI.1939-04.2004
649	Salas, R., Sturm, R., Boulter, J., & De Biasi, M. (2009). Nicotinic receptors in the habenulo-
650	interpeduncular system are necessary for nicotine withdrawal in mice. Journal of
651	Neuroscience, 29(10), 3014-3018. <u>https://doi.org/10.1523/JNEUROSCI.4934-08.2009</u>
652	Shih, P. Y., Engle, S. E., Oh, G., Deshpande, P., Puskar, N. L., Lester, H. A., & Drenan, R. M.
653	(2014). Differential Expression and Function of Nicotinic Acetylcholine Receptors in
654	Subdivisions of Medial Habenula. Journal of Neuroscience, 34(29), 9789-9802.
655	https://doi.org/10.1523/jneurosci.0476-14.2014
656	Soria-Gomez, E., Busquets-Garcia, A., Hu, F., Mehidi, A., Cannich, A., Roux, L., Louit, I.,
657	Alonso, L., Wiesner, T., Georges, F., Verrier, D., Vincent, P., Ferreira, G., Luo, M., &
658	Marsicano, G. (2015). Habenular CB1 Receptors Control the Expression of Aversive
659	Memories. Neuron, 88(2), 306-313. <u>https://doi.org/10.1016/j.neuron.2015.08.035</u>
660	Trifonov, S., Houtani, T., Hamada, S., Kase, M., Maruyama, M., & Sugimoto, T. (2009). In situ
661	hybridization study of the distribution of choline acetyltransferase mRNA and its splice
662	variants in the mouse brain and spinal cord. Neuroscience, 159(1), 344-357.
663	https://doi.org/10.1016/j.neuroscience.2008.12.054
664	Tuesta, L. M., Chen, Z., Duncan, A., Fowler, C. D., Ishikawa, M., Lee, B. R., Liu, XA., Lu, Q.,
665	Cameron, M., Hayes, M. R., Kamenecka, T. M., Pletcher, M., & Kenny, P. J. (2017).
666	GLP-1 acts on habenular avoidance circuits to control nicotine intake. Nature
667	Neuroscience, 20(5), 708-716. <u>https://doi.org/10.1038/nn.4540</u>

668	Varoqui, H., Schäfer, M. K. H., Zhu, H., Weihe, E., & Erickson, J. D. (2002). Identification of the
669	differentiation-associated Na+/PI transporter as a novel vesicular glutamate transporter
670	expressed in a distinct set of glutamatergic synapses. Journal of Neuroscience, 22(1),
671	142-155. https://doi.org/10.1523/jneurosci.22-01-00142.2002
672	Vong, L., Ye, C., Yang, Z., Choi, B., Chua, S., & Lowell, B. B. (2011). Leptin Action on
673	GABAergic Neurons Prevents Obesity and Reduces Inhibitory Tone to POMC Neurons.
674	Neuron, 71(1), 142-154. https://doi.org/10.1016/j.neuron.2011.05.028
675	Wallace, M. L., Huang, K. W., Hochbaum, D., Hyun, M., Radeljic, G., & Sabatini, B. L. (2020).
676	Anatomical and single-cell transcriptional profiling of the murine habenular complex.
677	Elife, 9. https://doi.org/10.7554/eLife.51271
678	Wang, T. W., Gentzke, A. S., Creamer, M. R., Cullen, K. A., Holder-Hayes, E., Sawdey, M. D.,
679	Anic, G. M., Portnoy, D. B., Hu, S., Homa, D. M., Jamal, A., & Neff, L. J. (2019).
680	Tobacco Product Use and Associated Factors Among Middle and High School Students
681	— United States, 2019. MMWR. Surveillance Summaries, 68(12), 1-22.
682	https://doi.org/10.15585/mmwr.ss6812a1
683	Wittenberg, R. E., Wolfman, S. L., De Biasi, M., & Dani, J. A. (2020). Nicotinic acetylcholine
684	receptors and nicotine addiction: A brief introduction. Neuropharmacology, 177, 108256.
685	https://doi.org/10.1016/j.neuropharm.2020.108256
686	Wolfman, S. L., Gill, D. F., Bogdanic, F., Long, K., Al-Hasani, R., McCall, J. G., Bruchas, M. R.,
687	& McGehee, D. S. (2018). Nicotine aversion is mediated by GABAergic interpeduncular
688	nucleus inputs to laterodorsal tegmentum. Nature communications, 9(1), 2710.
689	https://doi.org/10.1038/s41467-018-04654-2

Yamaguchi, R., Nicholson Perry, K., & Hines, M. (2014). Pain, pain anxiety and emotional and behavioural problems in children with cerebral palsy. *Disabil Rehabil, 36*(2), 125-130. <u>https://doi.org/10.3109/09638288.2013.782356</u>
Zell, V., Steinkellner, T., Hollon, N. G., Warlow, S. M., Souter, E., Faget, L., Hunker, A. C., Jin, X., Zweifel, L. S., & Hnasko, T. S. (2020). VTA Glutamate Neuron Activity Drives Positive Reinforcement Absent Dopamine Co-release. *Neuron, 107*(5), 864-873. <u>https://doi.org/10.1016/j.neuron.2020.06.011</u>

Zhang, J., Tan, L., Ren, Y., Liang, J., Lin, R., Feng, Q., Zhou, J., Hu, F., Ren, J., Wei, C., Yu, T.,
Zhuang, Y., Bettler, B., Wang, F., & Luo, M. (2016). Presynaptic Excitation via GABAB
Receptors in Habenula Cholinergic Neurons Regulates Fear Memory Expression. *Cell*, *166*(3), 716-728. <u>https://doi.org/10.1016/j.cell.2016.06.026</u>

701 Zhao-Shea, R., DeGroot, S. R., Liu, L., Vallaster, M., Pang, X., Su, Q., Gao, G., Rando, O. J.,

702 Martin, G. E., George, O., Gardner, P. D., & Tapper, A. R. (2015). Increased CRF

703 signalling in a ventral tegmental area-interpeduncular nucleus-medial habenula circuit

induces anxiety during nicotine withdrawal. *Nat Commun*, *6*, 6770.

705 <u>https://doi.org/10.1038/ncomms7770</u>

706 Zhao-Shea, R., Liu, L., Pang, X., Gardner, P. D., & Tapper, A. R. (2013). Activation of

GABAergic neurons in the interpeduncular nucleus triggers physical nicotine withdrawal
 symptoms. *Current Biology*, 23(23), 2327-2335.

709 https://doi.org/10.1016/j.cub.2013.09.041

710

711

712 FIGURE LEGENDS

713

714	Figure 1. Conditional knock-out of Slc17a7 (VGLUT1) from cholinergic neurons in MHb.
715	(a) Schematic of Kiaa ^{Cre} ; Rosa26 ^{ZSGreen} reporter mouse line with Cre expression driven by
716	Kiaa1107 regulatory elements and ZsGreen expression dependent on Cre recombination. (b)
717	Native ZsGreen fluorescence counterstained with DAPI in MHb (outlined); scale 200 $\mu\text{m.}$ (c)
718	Schematic of Cre recombination of the floxed Slc17a7 (VGLUT1) locus in the cKO (Kiaa ^{Cre} ;
719	SIc17a7 ^{flox/flox}) mouse line. (d) Fluorescent in situ hybridization of Cre, Chat, and SIc17a7
720	expression in MHb of control and cKO mice at two Bregma points; scale 100 $\mu\text{m}.$ (e) Higher
721	magnification images from white squares in (d); scale 50 $\mu\text{m}.$ Densitometric quantification
722	(without background subtraction) in ventral and dorsal MHb of (f) Cre, (g) Slc17a7 (VGLUT1),
723	and (h) Chat signals. Only Slc17a7 was significantly reduced in ventral MHb of cKO
724	(**p=0.006); n=3 mice per group.
725	
726	Figure 2: Loss of VGLUT1 in central IPN of cKO mice.
727	(a) Immunohistochemistry for ChAT, VGLUT1, and VGLUT2 in the IPN of control (Slc17a7 ^{flox})
728	and cKO mice (<i>Kiaa^{Cre}; Slc17a7^{flox/flox}</i>); bottom row shows ChAT and VGLUT1 merge; scale 100
729	$\mu\text{m}.$ Densitometric quantification (without background subtraction) in central and lateral IPN of
730	(b) ChAT, (c) VGLUT1, and (d) VGLUT2 signals. Only VGLUT1 was significantly reduced in

- cKO and only in the central IPN (***p*=0.0040); n=4 mice per group.
- 732

733 Figure 3: VGLUT2-expressing projections from MHb to IPN.

- 734 (a) Fluorescent in situ hybridization from Kiaa^{Cre} mouse showing Cre and Slc17a6 expression in
- the MHb (outlined); scale 100 μm. (b) High-resolution image showing expression of Cre,
- 736 SIc17a6 (VGLUT2), and DAPI in MHb of Kiaa^{Cre} mouse; scale 10 μm. Yellow arrows indicate

737some of the cells containing both *Cre* and *Slc17a6* mRNA. (c) Image of MHb from *Slc17a6*
Cre738(VGLUT2) mouse injected with AAV1-Ef1α-DIO-ChR2:mCherry bilaterally into the MHb739(outlined); scale 100 µm. (d) Immunohistochemistry of IPN from *Slc17a6*
Cre (VGLUT2-Cre)740mouse injected bilaterally with AAV1-Ef1α-DIO-ChR2:mCherry in MHb. VGLUT2
Cre MHb741terminals in IPN represented by mCherry+ expression, stained with VGLUT1 and ChAT; scale742100 µm.

744 Figure 4: Reduced glutamate transmission from MHb to IPN in VGLUT1 cKO mice.

745 (a) Schematic of electrophysiological preparation, with bilateral injections of AAV1-Ef1 α -DIO-

746 ChR2:mCherry in MHb of control (*Kiaa*^{Cre}) or cKO (*Kiaa*^{Cre}; *Slc17a7*^{flox/flox}) mice. Slice recordings

vising optogenetic stimulation performed in the IPN 3+weeks after injection. (b) Images from

748 control mouse of native Cre-dependent mCherry fluorescence in MHb (left) and fibers in IPN

749 (center, right); scale 100 μm. (c) Whole-cell recordings in IPN with single-pulse optogenetic

750 stimulation of MHb terminals led to oEPSC amplitudes that were reduced in the cKO (left,

751 ** p=0.001). Representative traces before and after DNQX in control (black) and cKO (blue)

752 (right). (d) oEPSC amplitude following train stimulation (1s) did not differ significantly different

753 between control and cKO groups (left). Representative traces before and after mecamylamine in

right, control (black) and cKO (blue) (right). Note that bars in panel c and d represent mean +/- SEM,

individual cells are represented by gray circles (control) or blue squares (cKO).

756

757 Figure 5: Increased nicotine self-administration in cKO mice.

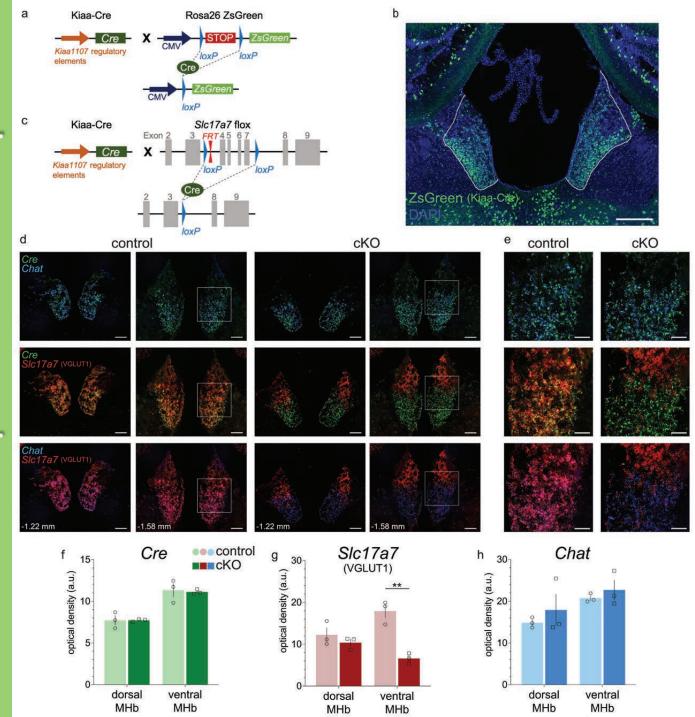
758 (a) Total distance traveled (*left*) and distance travelled across test segments (*right*) in open field

assay showed no significant differences between genotype. (b) Total time in center (*left*) and

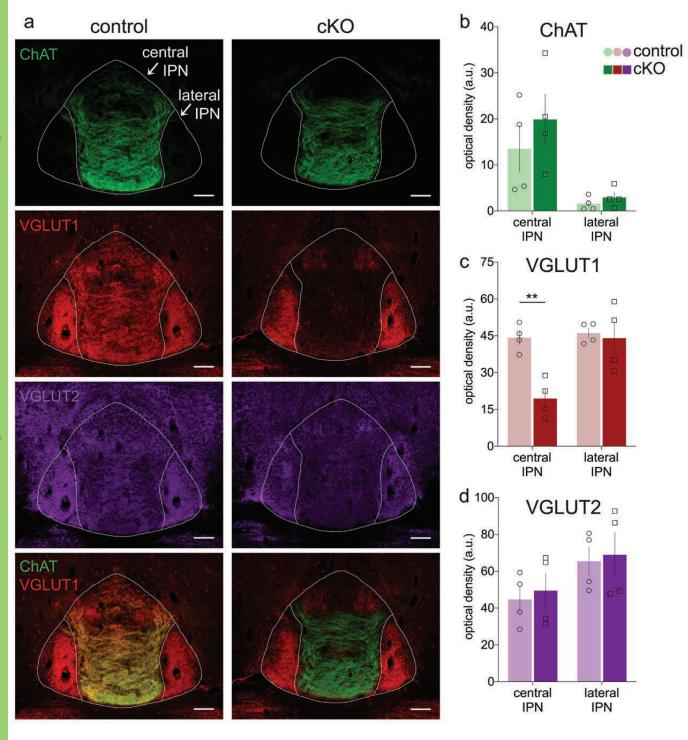
time in center across test segments (*right*) did not differ between genotype. (c) Active and

761 inactive lever presses during food training across test session did not differ by genotype. (d)

- 762 Active and inactive lever presses for nicotine show increased self-administration for cKO mice
- 763 (Sidak's *p<0.05, ***p<0.001). (e) cKO mice earned more total nicotine infusions in first 3
- nicotine test sessions (t-test, *p<0.05). (f) Nicotine infusions earned by control and cKO mice in
- 765 dose-response paradigm (*Sidak's, **p<0.005*).



eNeuro Accepted Manuscript



eNeuro Accepted Manuscript

